NANO EXPRESS

Sulfur Nanoparticles Synthesis and Characterization from H_2S Gas, Using Novel Biodegradable Iron Chelates in W/O Microemulsion

**Aniruddha S. Deshpande · Ramdas B. Khomane ·
Bhalchandra K. Vaidya · Renuka M. Joshi ·
Arti S. Harle · Bhaskar D. Kulkarni**

Abstract Sulfur nanoparticles were synthesized from hazardous H_2S gas using novel biodegradable iron chelates in w/o microemulsion system. Fe^{3+}–malic acid chelate (0.05 M aqueous solution) was studied in w/o microemulsion containing cyclohexane, Triton X-100 and *n*-hexanol as oil phase, surfactant, co-surfactant, respectively, for catalytic oxidation of H_2S gas at ambient conditions of temperature, pressure, and neutral pH. The structural features of sulfur nanoparticles have been characterized by X-ray diffraction (XRD), transmission electron microscope (TEM), energy dispersive spectroscopy (EDS), diffused reflectance infra-red Fourier transform technique, and BET surface area measurements. XRD analysis indicates the presence of α-sulfur. TEM analysis shows that the morphology of sulfur nanoparticles synthesized in w/o microemulsion system is nearly uniform in size (average particle size 10 nm) and narrow particle size distribution (in range of 5–15 nm) as compared to that in aqueous surfactant systems. The EDS analysis indicated high purity of sulfur (>99%). Moreover, sulfur nanoparticles synthesized in w/o microemulsion system exhibit higher antimicrobial activity (against bacteria, yeast, and fungi) than that of colloidal sulfur.

Introduction

Sulfur finds extensive technological applications such as in production of sulfuric acid, plastics, enamels, antimicrobial agent, insecticide, fumigant, metal glass cements, in manufacture of dyes, phosphate fertilizers, gun-powder and in the vulcanization of rubber, etc. [1–4]. Sulfur nanostructures are also used in synthesis of sulfur nanocomposites for lithium batteries [5, 6], modification of carbon nanostructures [7, 8], in synthesis of sulfur nanowires with carbon to form hybrid materials with useful properties for gas sensor and catalytic applications [9], Metal-sulfur compounds like ZnS and CdS play important role in non-linear optical and electroluminescent devices, etc. [10–15].

The synthesis of nanoparticles can be carried out by various methods. Among them, use of microemulsion system is an attractive and simple method as it allows greater control over nanoparticle morphology (size and shape) [16, 17]. Recently, Guo et al. [18] reported the synthesis of monoclinic sulfur nanoparticles using the mixture of two w/o microemulsion systems. However, during synthesis the H_2S gas was released as hazardous by-product. In this study we report for the first time synthesis of sulfur nanoparticles in the range of 5–15 nm from H_2S gas by catalytic conversion using biodegradable iron chelates in w/o microemulsion system.

The catalytic conversion of H_2S gas to elemental sulfur can be achieved by various chemical [19–22] and

A. S. Deshpande · R. B. Khomane · B. K. Vaidya ·
R. M. Joshi · B. D. Kulkarni (✉)
Chemical Engineering & Process Development Division,
National Chemical Laboratory, Dr. Homi Bhabha Road,
Pune 411008, India
e-mail: bd.kulkarni@ncl.res.in

A. S. Deshpande
e-mail: as.deshpande@ncl.res.in;
aniruddhadesh@rediffmail.com

A. S. Harle
Center for Material Characterization Division,
National Chemical Laboratory, Dr. Homi Bhabha Road,
Pune 411008, India

biological [23, 24] means for gas sweetening. Nagal [25] has reported the gas desulfurization based on liquid redox chemistry, as follows

$$H_2S_{(g)} + H_2O_{(l)} \leftrightarrow H_2S_{(l)}, \tag{1}$$

$$H_2S_{(l)} + 2Fe^{3+} L^{n-}_{(1)*} \rightarrow S^0 \downarrow + 2H^+ + 2Fe^{2+} L^{n-}_{(1)}, \tag{2}$$
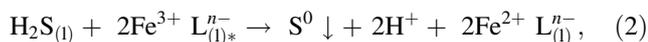
where 'L' denotes an organic ligand, which are usually a polyaminocarboxyllic acid, such as ethylenediamine tetraacetic acid (EDTA), nitrilotriacetic acid (NTA), hydroxy, diethylenetriamine pentaacetic acid (DTPA), etc. [26] and 'n' denotes the charge on the organic ligand. Since the active ferric chelate is converted to inactive ferrous chelate, the later component has to be regenerated by oxidation according to the reactions,

$$\tfrac{1}{2} O_{2(g)*} + H_2O_{(l)} \leftrightarrow \tfrac{1}{2} O_{2(l)}, \tag{3}$$

$$2Fe^{2+}L^{n-}_{(1)} + \tfrac{1}{2}O_{2(l)} + H_2O_{(l)} \rightarrow 2Fe^{3+}L^{n-}_{(1)} + OH^- \tag{4}$$
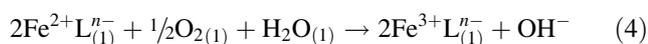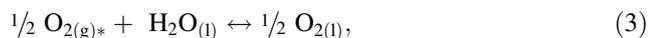
At present, use of iron chelates has been extensively commercialized in Lo-CAT, Sulferox process [27]. However, these chelating agents (e.g., EDTA, DTPA, NTA, Cyclohexane-1,2-diaminetetraacetic (CDTA), etc.) have very low rate of biodegradation and therefore cause environmental pollution. Alternative chelating agents for gas sweetening should meet three main criteria, viz. (1) should possess equal to or better complex forming properties compared to commercial chelating agents, (2) should possess better biodegradability, and (3) should contain low nitrogen to minimize the nitrogen content in effluents. It has been reported that carboxylic acids (e.g., citric acid, malic acid, gluconic acid, etc.) have good chelating properties and have faster rate of biodegradation [28, 29].

In this study use of novel biodegradable iron chelates, in particular FeCl$_3$–malic acid chelate system, has been extensively studied in w/o microemulsion (cyclohexane/n-hexanol/Triton X-100/water) for the catalytic conversion of H$_2$S gas to sulfur nanoparticles. The sulfur nanoparticles have been systematically characterized by X-ray diffraction (XRD), transmission electron microscope (TEM), energy dispersive

spectroscopy (EDS), diffused Reflectance Infra-red Fourier transform technique (DRIFT-IR), and BET surface area measurements. Furthermore, the potency of antimicrobial activity of sulfur nanoparticles has been determined by plate assay and compared with that of colloidal sulfur.

Materials and Methods

Materials

All chemicals were of analytical grade and used without further purification. Ferric chloride, ferric sulfate, ferric nitrate, gluconic acid, malic acid, citric acid, sodium hydroxide, sodium sulfide, cyclohexane, n-hexanol, Triton X-100 were purchased from Merck India. All solutions were prepared by deionized milli-Q water (Q-H$_2$O with 18.2 MQ cm resistivity, Millipore corporation).

All microbial cultures (*Pseudomonas areuginosa* NCIM 2036 and *Styphylococcus areus* NCIM 2079; *Candida albicans* NCIM 3102, *C. albicans* NCIM 3466, *Aspergillus flavus* NCIM 535, and *Aspergillus niger* 545) were procured from National Collection of Industrial Micro-organisms (NCIM), NCL-Pune (India).

Preparation of Iron Chelate Solution

Iron chelates were synthesized using ferric salts (*namely* ferric chloride, ferric sulfate, and ferric nitrate) in combination with different carboxylic acids (*namely* monodenatate gluconic acid, bidenatate malic acid, and tridenatate citric acid) as a chelating agent in various molar ratios as given in Table 1. These iron chelates were used in the concentration range of 500–20,000 ppm iron for catalytic conversion of H$_2$S to elemental sulfur at ambient conditions of temperature, pressure and pH 7–7.5. FeCl$_3$–malic acid chelate was found to give elemental sulfur of high purity and better recovery and has therefore been selected for further studies.

Table 1 Screening of iron chelate systems

Iron salt	Chelating agent	Molar ratio	Reaction time (min)	Sulfur recovered mg/gm of iron chelate	% purity Sulfur[a]
FeCl$_3$	Citric acid	1:2	36	184.20	>99
	Malic acid	1:3	15	499	>99
	Gluconic acid	1:3	5	27.7	83.71
Fe$_2$(SO$_4$)$_3$	Citric acid	1:2	25	137.8	97.5
	Malic acid	1:3	37	235	>99
	Gluconic acid	1:3	39	51	88.44
Fe$_2$(NO$_3$)$_3$	Citric acid	1:2	10	116,83	75.96
	Malic acid	1:3	5	290.88	94
	Gluconic acid	1:3	20	90	99

[a] The precipitate besides sulfur also contains C, N, H, and Fe, etc., as shown by elemental analysis

General Method of Sulfur Recovery from H₂S Gas

Figure 1 shows schematic flow diagram for catalytic conversion of H_2S to elemental sulfur. Pure H_2S gas (99.9%) was sparged in the absorber unit for about 35–45 min. In the absorber unit, Fe^{3+}–malic acid chelate solution oxidized H_2S gas to elemental sulfur and simultaneously active ferric chelate was reduced to inactive ferrous chelate (reaction 2). After complete reduction of ferric chelate, H_2S conversion to elemental sulfur ceases. The outlet gas from absorber unit was checked intermittently by formation of black precipitate of Ag_2S on bubbling through 0.1 N $AgNO_3$ solution. The regeneration of inactive ferrous chelate to active ferric chelate was carried out by sparging pure oxygen (reaction 4). The regenerated ferric chelate was recycled for further H_2S conversion.

Synthesis of Sulfur Nanoparticles

Preparation of FeCl₃–malic acid (Fe³⁺–malic acid) Chelate Solution

Iron chelate solution (0.05 M) was prepared by dissolving ferric chloride and malic acid (1:3 mole ratio) in deionized water. The pH of the solution was adjusted to 7.0–7.5 with sodium hydroxide solution. This aqueous chelate solution was used in the w/o microemulsion system for synthesis of sulfur nanoparticles.

Synthesis of Sulfur Nanoparticles in W/O Microemulsion System

The oil phase was prepared by mixing 52 wt.% of cyclohexane, 22 wt.% Triton X-100 (as surfactant), and 11 wt.% n-hexanol (as co-surfactant) under constant stirring. Then 15% (0.05 M) aqueous Fe^{3+}–malic acid chelate solution

was added drop wise to the oil phase under vigorous stirring in order to prepare optically clear and stable system. The sulfur nanoparticles synthesis was carried out by the procedure described earlier in section "General method of sulfur recovery from H_2S gas." The oxidation of H_2S occurred inside aqueous micelle containing iron chelate as shown in Fig. 2. The precipitated sulfur was separated by centrifugation at 8,000 rpm for 20 min and washed with water, methanol, and dried under vacuum at 60 °C for 4 h.

Instrumentation

The sulfur nanoparticles were characterized by XRD using Rigaku Dmax 2500 diffractometer equipped with graphite monochromatized CuKa radiation ($\lambda = 1.5406$ Å) employing a scanning rate of 5°/min in the 2θ range from 10 to 80°. The EDS was carried out by using EDAX of Phoenix Company. The morphology of the sulfur nanoparticles was observed by TEM. The samples for TEM analysis were prepared by deposition of an ultrasonically dispersed suspension of the sulfur product in methanol on collidon and carbon-coated copper grids. The TEM measurements were performed on a JEOL model 1200EX instrument. Infrared (IR) spectra were recorded by Parkin-Elmer system 2000 Infrared spectroscope employing a potassium bromide (KBr) using DRIFT-IR.

Evaluation of Antimicrobial Activity of Sulfur Nanoparticles

The antimicrobial activity of sulfur nanoparticles was determined by plate assay and compared with that of colloidal sulfur. Here, nutrient agar (HiMedia, India), MGYP [malt extract (0.3 g), glucose (1.0 g), yeast extract (0.3 g), peptone (0.5 g), and agar (2.0 g/100 mL medium)], and potato dextrose agar (HiMedia, India) were used as growth

Fig. 1 Simplified process flow diagram for catalytic conversion of H₂S to elemental sulfur (1, H₂S cylinder; 2, O₂ cylinder; 3, bomb; 4, gas inlet; 5, absorber/regenerator; 6, outlet gas checking port; 7, sulfur recovery; 8, gas inlet; 9, NaOH scrubber; 10, sweet gases; V1–V9, valves)
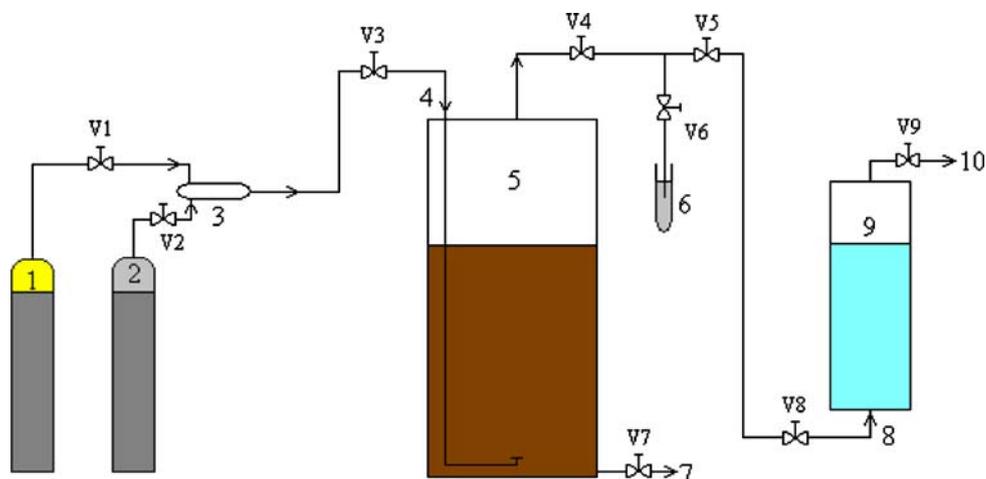
Fig. 2 Schematic representation of synthesis of sulfur nanoparticles in w/o microemulsion system

Reaction – 2

$$H_2S_{(g)} + 2Fe^{3+} L^{n-}_{(l)} \rightarrow S^0 \downarrow + 2H^+ + 2Fe^{2+} L^{n-}_{(l)}$$

Reaction – 4

$$2 Fe^{2+} L^{n-}_{(l)} + \tfrac{1}{2} O_{2(l)} + H_2O_{(l)} \rightarrow 2 Fe^{3+} L^{n-}_{(l)} + OH^-$$
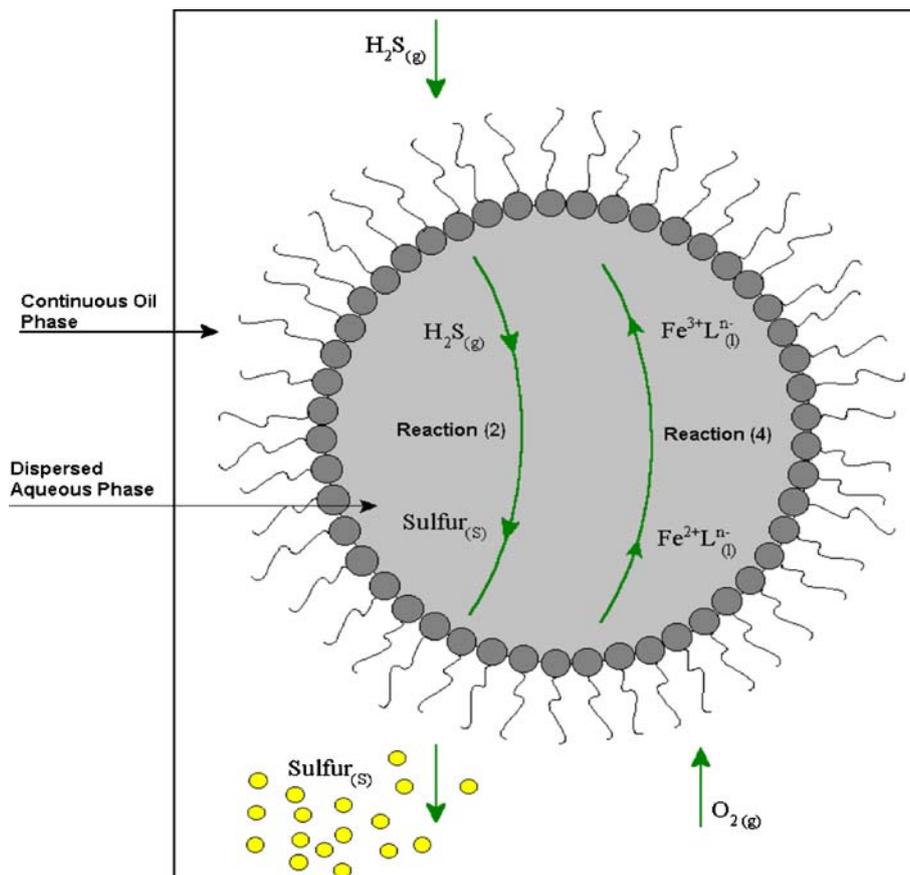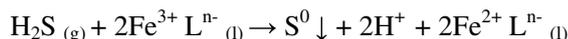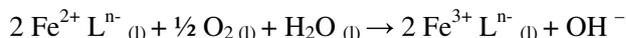
media for bacterial, yeast, and fungal strains, respectively. The antimicrobial activity of sulfur nanoparticles and colloidal sulfur was determined by measuring the inhibition zones on agar plates inoculated with bacterial (*P. areuginosa*, *S. areus*), yeast (*C. albicans*), and fungal strains (*A. flavus*, *A. niger*). An aliquot part of 0.5 mL freshly prepared microbial cell suspension was added on sterile Petri plates containing solidified agar medium. An aliquot part of 30 μL of sulfur suspension was added on agar plates followed by incubation at specified temperature (28 °C for yeast and fungi, 30 °C for bacteria). Being antimicrobial agent, sulfur inhibited the growth of microorganism and inhibition zones were formed. The inhibition zones were measured after 24 h for bacteria and after 48 h for yeast and fungi. The efficiency of antimicrobial activity is expressed in terms of average diameter of inhibition zones obtained by triplicate results.

Results and Discussion

Selection of Optimum Iron Chelate System

Different iron chelates were evaluated for catalytic conversion of H_2S gas to elemental sulfur. Table 1 reports the values of reaction time indicating the breakthrough of H_2S uptake since the beginning of experiments. In all experiments, the volume of the reaction mixture and the rate of H_2S gas addition were kept constant. The values of 'reaction time' therefore give a measure of the rate of reaction for various iron chelates. Besides the reaction time, purity and recovery of sulfur also need to be considered to establish the best iron chelate system. Among various iron chelates, $FeCl_3$–gluconic acid chelate system required much less reaction time than the others (5 min); however, the purity and recovery of product was very poor. Over all,

FeCl$_3$–malic acid chelate system has been observed to give maximum recovery of sulfur (499 mg/g of iron chelate) along with high purity (>99%) and reasonable extent of reaction time (15 min). Hence it was selected for further evaluation in w/o microemulsion system.

XRD Analysis of the Sulfur Particles

The XRD analysis of sulfur nanoparticles synthesized in w/o microemulsion and aqueous solution is shown in Fig. 3. The position and intensities of the diffraction peaks of all samples were compared with standard α-sulfur particle diffraction pattern [30].

The presence of sharp peaks in Fig. 3b (and in the insight) indicates highly crystalline nature of the sulfur nanoparticles synthesized using w/o microemulsion system compared to particle synthesized by normal aqueous phase (Fig. 3a). The determination of the mean particle diameter (D) was done by the XRD analysis using Debye-Scherrer formula,

$$D = \frac{k\lambda}{\beta \cos \theta} \qquad (5)$$

where D is the crystallite size, k the Scherrer constant usually taken as 0.89, λ the wavelength of the X-ray radiation (0.154056 nm for Cu Kα), and β is the full width at half maximum of the diffraction peak measured at 2θ.

The estimated crystallite size of the sample prepared in microemulsion from line broadening of the most intense diffraction peak is approximately 10 nm.

EDS Analysis

The synthesized nanoparticles were characterized by EDAX for the evaluation of their composition and purity. Figure 4 shows the spectrum of the EDAX analysis. It is evident from the peaks that the product is completely pure and corresponds to sulfur element only, which are synthesized in w/o microemulsion system and aqueous system.

TEM Analysis

The morphology of the sulfur nanoparticles synthesized in w/o microemulsion system and aqueous system was analyzed using TEM (Fig. 5). Sulfur particles prepared in aqueous phase showed larger particle size and a wider particle size distribution ($\sim$80–100 nm) (Fig. 5a), However, sulfur nanoparticles synthesized in w/o microemulsion system show very fine particle size ($\sim$10 nm) and a relatively narrow particle size distribution ($\sim$5–15 nm) (Fig. 5b). Figure 6 shows the histogram for the sulfur nanoparticles size distribution synthesized in W/O microemulsion.

Fig. 3 XRD of sulfur particle synthesis in: (**a**) aqueous phase; (**b**) w/o microemulsion
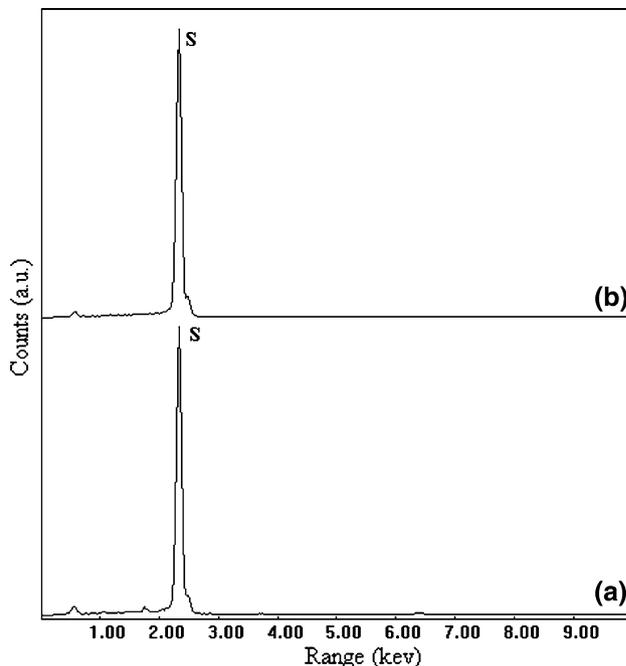
Fig. 4 EDAX of sulfur nanoparticles synthesized in: (**a**) aqueous phase; (**b**) w/o microemulsion

Fig. 5 TEM analysis for sulfur nanoparticles synthesized in different systems: (**a**) aqueous phase system; (**b**) w/o microemulsion
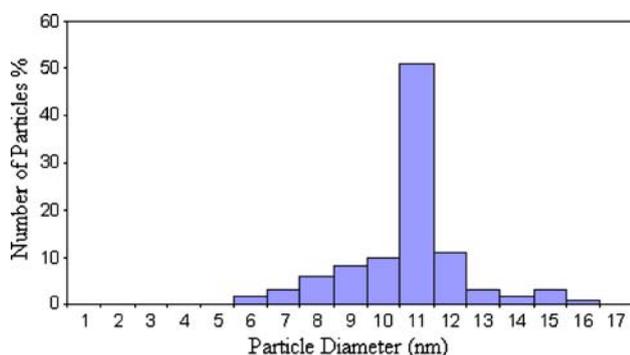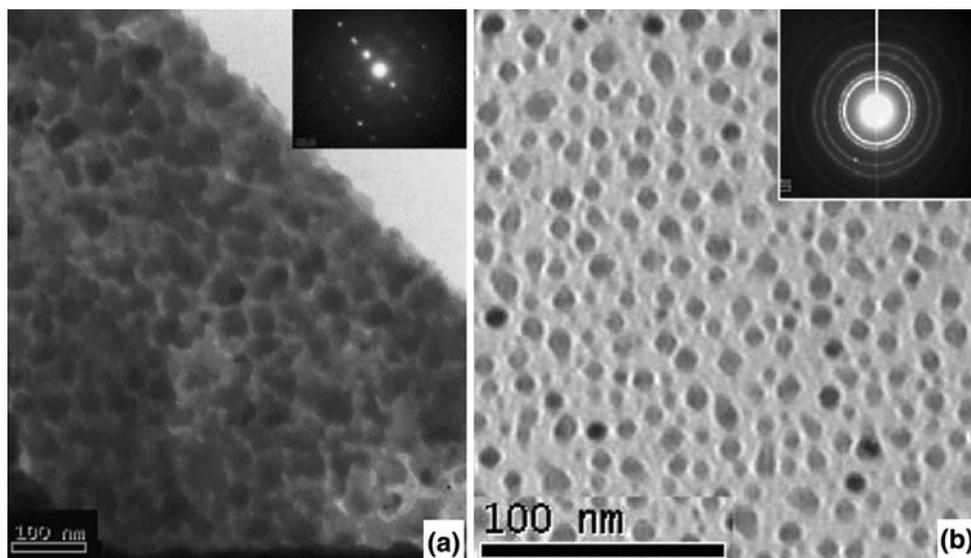
Fig. 6 Histogram for particles size distribution for sulfur nanoparticles synthesized in w/o microemulsion

Fig. 7 Diffused reflectance infra-red Fourier transform analysis: (**a**) sulfur nanoparticles; (**b**) Std IR of rhombic sulfur

IR Analysis

Figure 7 shows DRIFT-IR analysis of standard α-sulfur and nanoparticles synthesized using w/o microemulsion system. The IR spectrum of the sulfur nanoparticles (Fig. 7a) indicate presence of all characteristic peaks of α-sulfur at 463(s), 505(w), 550(m), 590(m), 617(m), 656(s), 683(m), 710(m), 845(s), 876(m), 903(m), 936(m), 986(w), 1,052(w), 1,298(m), 1,513(m) cm^{-1} when compared with standard α-sulfur (Fig. 7b) [31].

Antimicrobial Activity of Sulfur Nanoparticles

The sulfur element is known to possess potent antimicrobial activity [4]. Due to their smaller particle size (~ 10 nm), sulfur nanoparticles are expected to exhibit antimicrobial action at lower concentrations than sulfur particles synthesized in aqueous phase (80–100 nm). Furthermore, BET analysis shows that there was significant increase in surface area of sulfur nanoparticles (177 m^2/g)

compared to sulfur (48 m^2/g) synthesized in aqueous phase only as shown in BET isotherms as shown in Figs. 8 and 9, respectively.

The results of antimicrobial activities of nanoparticle and sulfur are summarized in Table 2. The inhibition zones for bacteria and yeast were determined at 30 and 150 μg/mL of sulfur suspension. In bacterial strains, sulfur nanoparticles gave larger inhibition zones compared to that of sulfur. Similarly, sulfur nanoparticles were found to be more effective than sulfur in inhibiting growth of yeasts strains (*C. albicans* NCIM 3102 and 3466). This indicates that at the same concentration, the sulfur nanoparticles have better

Fig. 8 BET isotherm for the sulfur nanoparticles synthesized in w/o microemulsion
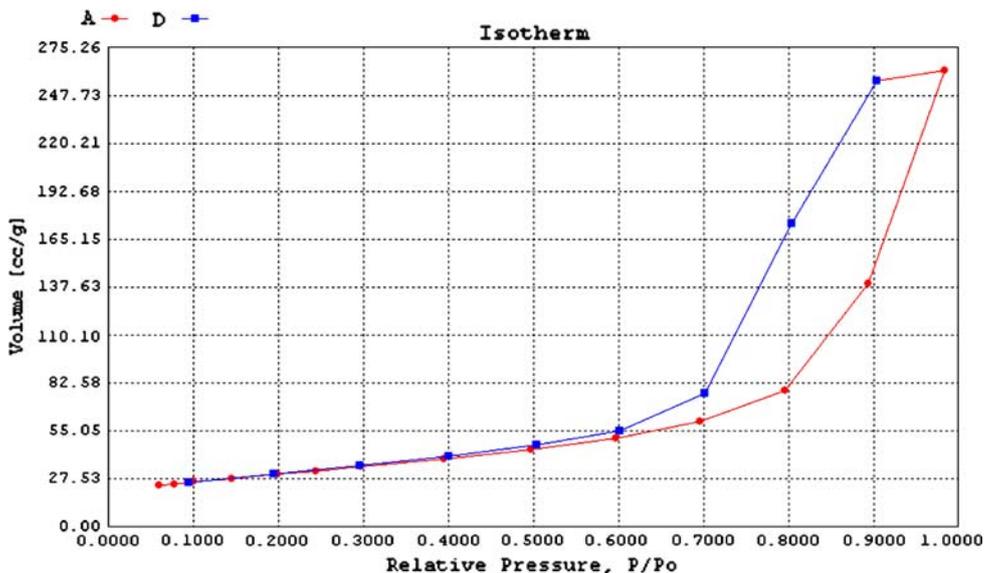
antimicrobial activity against bacterial and yeast cultures than that of sulfur.

In case of Fungi, 30 and 150 µg/mL suspensions of sulfur gave no inhibition zones. Therefore the antifungal activity was determined at higher concentrations. The distinct inhibition zones were observed when sulfur nanoparticles concentration was increased up to 1,500 and 3,000 µg/mL (Table 2). In the case of *A. niger*, sulfur nanoparticles (at 1,500 and 3,000 µg/mL concentrations) were found to retard normal fungal growth. Here the formation of spores (late stage of fungus growth cycle) was observed to be delayed by about 48 h. Thus the reduction in particle size enhances the effectiveness of sulfur particles as antimicrobial agent. These results are significant and indicate the greater efficacy of sulfur nanoparticles than normal sulfur particularly as an antifungal agent.

To the best of our knowledge, the detail study of iron chelating property of malic acid has not yet been reported. Due to low biodegradability (e.g., BOD_5 of EDTA: 0.01%), the disposal of iron chelates used in Lo-CAT process raised serious environmental concern [28]. In order to overcome this environmental pollution, there is need to look for alternative iron chelating agents. The carboxylic acids are known to possess high rate of biodegradation (e.g., BOD_5 of malic acid: 65%) along with good iron chelating property. The results of the present investigation indicated that Fe^{+3}–malic acid iron chelates in w/o microemulsion can effectively oxidize hazardous H_2S gas to produce sulfur nanoparticles. Besides reduction in environmental pollution (use of biodegradable chelating agents) and waste utilization (H_2S abatement), the described process also has high commercial significance.

Fig. 9 BET isotherm for the sulfur synthesized in aqueous phase only
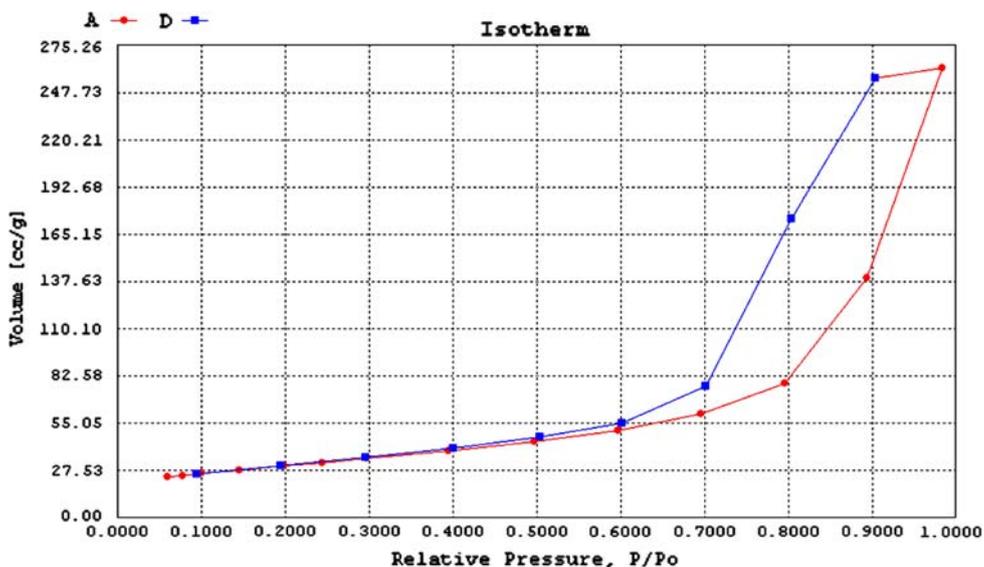
Table 2 Antimicrobial activity of sulfur nanoparticles

Type of micro-organism	Microbial strain (µg/mL)	Zone of inhibition (mm)	
		Sulfur synthesized in aqueous system (80–100 nm)[a]	Sulfur nanoparticles (5–15 nm)[a]
Bacteria	*P. areuginosa* NCIM 2036		
	(i) 30	Nil	7.3
	(ii) 150	8.7	25
	S. areus NCIM 2079		
	(i) 30	Nil	7.7
	(ii) 150	Nil	30
Yeast	*C. albicans* NCIM 3102		
	(i) 30	Nil	8.3
	(ii) 150	7.1	10
	C. albicans NCIM 3466		
	(i) 30	Nil	8.3
	(ii) 150	7.3	11
Fungi	*A. spergillus flavus* NCIM 535		
	(i) 1,500	Nil	14
	(ii) 3,000	Nil	22.5
	A. niger NCIM 545		
	(i) 1,500	Nil	Growth retardation[b]
	(ii) 3,000	Nil	Growth retardation[b]

[a] Average particle size

[b] Formation of spores was observed to be delayed by about 48 h

Conclusions

Synthesis of α-sulfur nanoparticles by catalytic oxidation of H_2S gas using biodegradable Fe^{+3}–malic acid chelate system in w/o microemulsion has been reported first time. The described process gives highly crystalline pure α-sulfur with uniform shape and size of 10 nm of sulfur nanoparticles. The synthesized nanoparticles are showing very high antimicrobial and antifungal activity compare to sulfur synthesized in aqueous phase only. The sulfur nanoparticles synthesis was carried out at ambient temperature and atmospheric pressure and between pH 7 and 7.5. The described process serves mainly two objectives: waste utilization for preparation of commercially important product and reduction in environmental pollution.

References

1. K.S. Leslie, G.W.M. Millington, N.J. Levell, J. Cosmet. Dermatol. **13**, 94 (2004)
2. Merck Index, 13th edn. (Merck & Co. Inc., USA, 2001), p. 1599
3. D.R. Lide, *CRC Handbook of Chemistry and Physics*, 85th edn. (CRC press, New York, 2004), p. 30
4. J.T. Weld, A. Gunther, J. Exp. Med. **85**, 531 (1946)
5. X. Yu, J. Xie, J. Yang, K. Wang, J. Power Sources **132**, 181 (2004)
6. W. Zheng, Y.W. Liu, X.G. Hu, C.F. Zhang, Electrochim. Acta **51**, 1330 (2006)
7. J. Barkauskas, R. Juskenas, V. Mileriene, V. Kubilius, Mater. Res. Bull. **42**, 1732 (2007)
8. E.A. Smorgonskaya, R.N. Kyutt, V.B. Shuman, A.M. Danishevskii, S.K. Gordeev, A.V. Grechinskaya, Phys. Solid State **44**, 1908 (2002)
9. P. Santiago, E. Carvajal, D. Mendoza, L. Rendon, Microsc. Microanal. **12**(suppl. 2), 690 (2006)
10. J. Xu, W. Ji, J. Mater. Sci. Lett. **2**, 115 (1999)
11. R.B. Khomane, A. Manna, A.B. Mandale, B.D. Kulkarni, Langmuir **18**, 8237 (2002)
12. A. Kumar, A. Jakhmola, J. Colloid. Interf. Sci. **297**, 607 (2006)
13. J. Zhu, Y. Zhu, M. Ma, L. Yang, L. Gao, J. Phys. Chem. C **111**, 3920 (2007)
14. L. Kienle, V. Duppel, S. Schlecht, Soild State Sci. **6**, 179 (2004)
15. P.P. Chin, J. Ding, J.B. Yi, B.H. Liu, J. Alloy. Compd. **390**, 255 (2005)
16. B.K. Paul, S.P. Moulik, Curr. Sci. **80**, 990 (2001)
17. S. Eriksson, U. Nylen, S. Rojas, M. Moutonnet, Appl. Catal. A Gen. **265**, 207 (2004)
18. Y. Guo, J. Zhao, S. Yang, K. Yu, Z. Wang, H. Zhang, Powder Technol. **162**, 83 (2006)
19. S.E. Jhon, Environ. Prog. **21**, 143 (2002)
20. T. Klaus, Chem. Eng. World **39**, 43 (2004)
21. W.C. Yu, G. Astarita, Chem. Eng. Sci. **42**, 418 (1987)
22. S. Asai, Y. Konishi, T. Yabu, AIChE J. **36**, 1331 (1990)
23. C. Pagella, D.M. De Faveri, Chem. Eng. Sci. **55**, 2185 (2000)

24. A.B. Jensen, C. Webb, Enzyme Microb. Technol. **17**, 2 (1995)
25. G. Nagal, Chem. Eng. **104**, 125 (1997)
26. J.F. Demmink, A. Mehra, A.A.C.M. Beenackers, Chem. Eng. Sci. **57**, 1723 (2002)
27. R.A. Pandey, S. Malhotra, Crit. Rev. Environ. Sci. Technol. **29**, 229 (1999)
28. V. Karel, Handbook of Environmental Data on Organic Chemicals, 3rd edn. (VanNostrand Reinhold an international Thomson Publishing Company, New York, 1996)
29. A.S. Deshpande, N.V. Sankpal, B.D. Kulkarni, Indian Patent, 1366/DEL/2003
30. Joint Commission on Powder Diffraction Standards. Powder diffraction file, Inorganic phase. International center for diffraction data. PA, USA. JCPDS No. 08247, p. 410
31. H.L. Strauss, J.A. Greenhouse, *Elemental Sulfur Chemistry and Physics* (Meyer, B. Interscience Publishers, New York, 1965), pp. 241–250